Microrheology and structure of a yield-stress polymer gel

Felix K. Oppong,[1,2] Laurent Rubatat,[3] Barbara J. Frisken,[3] Arthur E. Bailey,[3,4] and John R. de Bruyn[1,2]
[1]*Department of Physics and Physical Oceanography, Memorial University of Newfoundland, St. John's NF, Canada A1B 3X7*
[2]*Department of Physics and Astronomy, University of Western Ontario, London, Ontario, Canada N6A 3K7*
[3]*Department of Physics, Simon Fraser University, Burnaby, British Columbia, Canada V5A 1S6*
[4]*Scitech Instruments, North Vancouver, British Columbia, Canada V7J 2S5*
(Received 20 January 2006; published 14 April 2006)

The small-scale rheology of Carbopol ETD 2050, a polymer gel with a yield stress, is studied as a function of polymer concentration by measuring the diffusion of submicron-sized spherical fluorescent particles suspended in gel. Dynamic light scattering is used to determine the mean-squared displacement $\langle r^2(\tau)\rangle$ of the particles as a function of lag time τ. Fluorescence microscopy is used to track the particle trajectories directly, from which $\langle r^2(\tau)\rangle$ and the van Hove correlation function are determined. From our results we calculate the microrheological viscous and elastic moduli of the material. The two techniques cover complementary ranges of τ and $\langle r^2(\tau)\rangle$ and give results that agree well. The microrheological moduli are substantially smaller than the bulk values as determined by conventional shear rheometry. The bulk viscoelastic behavior is dominated by the elastic modulus, while at low enough concentrations and high enough frequencies the microrheological response is predominantly viscous. These results will be discussed in the context of the gel structure.

DOI: 10.1103/PhysRevE.73.041405 PACS number(s): 82.70.Dd, 83.60.−a

I. INTRODUCTION

Soft materials such as gels, foams, or emulsions are in general structured fluids, and their complex and fascinating properties result from their structure on scales much larger than that of individual molecules, but smaller than that of the bulk material [1]. This structure affects both the equilibrium and nonequilibrium properties of these materials and, in particular, their response to shear. Typically such materials are viscoelastic; that is, their response to shear includes both the dissipation (viscosity) and storage (elasticity) of energy. In some cases the structure of the fluid gives it sufficient strength to resist shear completely for small enough stress. Such materials, called viscoplastic or yield-stress fluids, behave as elastic solids at low stress but flow when the shear stress becomes larger than a yield stress; examples include mayonnaise and fresh concrete. It is clearly of interest to understand the microscopic structure and properties of yield-stress fluids and, in particular, to develop an understanding of the relationship between their microstructure and bulk properties.

In this paper, we report both macroscopic and microscopic measurements of the rheological properties of a model viscoplastic material, Carbopol ETD 2050. Carbopol is a family of commercial polymers based on cross-linked linear polyacrylic acid chains [2] that is used commercially to modify the rheological properties of cosmetic and pharmaceutical products. It is widely used as a model yield-stress fluid because of its stability and transparency [3–5]. Dispersions of Carbopol in water are described in the product literature [2] and elsewhere [3,6–10] as being made up of a collection of polymer gel particles covered with dangling polymer chains that interact strongly with neighboring particles, although it does not appear that systematic efforts have been made to determine the microscopic structure.

The rheological properties of Carbopol solutions depend primarily on concentration and *p*H. When dispersed in water at concentrations up to about 2% by weight, it forms a viscous sol with a low *p*H. Neutralization by the addition of alkali causes ionization along the polymer backbone, and the resulting electrostatic repulsion leads to the uncoiling and expansion of the non-cross-linked polymer chains. This in turn leads to swelling of the polymer and the formation of a stiff, transparent gel. The bulk rheological properties of dispersions of different grades of Carbopol have been reported as a function of *p*H and concentration and with different additives [3,9,11]. Neutralized Carbopol dispersions typically have a yield stress of tens of Pa at concentrations of a few tenths of a percent by weight.

There has recently been substantial effort directed towards the development of what are referred to as microrheological techniques, which probe the viscoelastic response of complex fluids on the microscopic scale. References [12–15] are recent reviews. There are several factors motivating this effort: microrheological methods require a smaller sample than conventional bulk rheological techniques, and they have the potential to probe the viscoelastic response of the sample at much higher frequencies than are accessible with conventional shear rheometry. In addition, some microrheological methods allow for the investigation of local rheological properties and so for the study of small-scale material inhomogeneities [16]. Many microrheological techniques, including dynamic light scattering [17], diffusing wave spectroscopy [17–20], and direct imaging and tracking of the trajectories of the tracer particles [21–24], involve the passive measurement of the mean-squared displacement $\langle r^2(\tau)\rangle$ of small (micron- or submicron-sized) particles suspended in the material as a function of lag time τ. Active techniques, on the other hand, involve measurement of the response of a small particle to an external force applied with, for example, a magnetic field [25–27] or optical tweezers [28–32].

Passive microrheology techniques rely on the diffusion of tracer particles, driven by thermal fluctuations, to probe the

viscoelastic properties of the materials [16–24,33–38]. The fluctuation-dissipation theorem links the mean-squared displacement of these particles to the linear viscoelastic response function of the material. If the characteristic length scale of the material structure is small compared to the particle size, then microrheological measurements lead to viscous and elastic moduli that agree with those obtained from bulk rheological measurements [17,18,35,36]. On the other hand, if the length scale of the material is larger than that of the particles, then the particle motion is sensitive to local inhomogeneities in the material properties. In this case microrheological measurements will differ from bulk measurements and provide information about the local structure of the fluid.

In this paper we use dynamic light scattering and direct particle tracking to study the microrheology of Carbopol gels, with the aim of exploring differences between bulk and microscopic properties in yield-stress fluids. In both cases we determine the mean-squared displacement $\langle r^2(\tau)\rangle$ of our tracer particles. In the case of light scattering, $\langle r^2(\tau)\rangle$ is calculated from the decay in time of the autocorrelation function of the scattered light intensity, while in the case of particle tracking it is obtained by averaging over the trajectories measured for a large number of particles. The two techniques complement each other: particle tracking gives information about the viscoelastic properties of the material at low frequencies (in our case, 0.005–60 Hz) and for length scales of the order of 0.1–3 μm, while dynamic light scattering covers frequencies from 1 to 10^4 Hz and length scales of 0.003–0.3 μm. Together, these two techniques allow us to probe the viscoelastic response of carbopol gels over more than six orders of magnitude in frequency. We compare our microrheological measurements with bulk values of the elastic and viscous moduli measured with a conventional shear rheometer and discuss the results in the context of the microstructure of Carbopol.

II. EXPERIMENT

A. Sample preparation

Our experiments were performed using Carbopol ETD 2050. This particular variety of Carbopol is constituted of homopolymers and copolymers of polyacrylic acid, crosslinked with a polyalkenyl polyether [10]. This material was chosen for the ease with which it can be dispersed in water and for the very high degree of transparency of the resulting gels. Sample preparation was done under ambient conditions in a dust-free fume hood. Polystyrene latex microspheres of diameter 0.49 μm, density 1.05 g/cm^3, refractive index 1.59 at 589 nm, and containing a dye which fluoresced in the red when excited with green light were provided as a suspension in water [39]. This suspension was sonicated in an ultrasonic bath to disperse any clumping. The spheres were then added to de-ionized water to give a volume fraction of typically 5×10^{-5} for particle tracking experiments or 1×10^{-5} for the light scattering experiments. The lower concentration in the latter case is needed to avoid multiple scattering of the laser light as it passes through the sample.

Carbopol powder was added over the course of several hours to the water/sphere suspension to a concentration of 1.2 wt % while stirring with a magnetic stirrer at approximately 20 rpm. The resulting dispersion had a *p*H of about 3. Sodium hydroxide solution at 15 wt % was then added to bring the *p*H up to 6. The gel samples used in this work were obtained by diluting the above stock solution with the appropriate amount of water containing the fluorescent spheres to get the desired Carbopol concentration c. Air bubbles in the gel were removed by centrifugation. Samples used for bulk rheological measurements did not include any fluorescent microspheres, but were otherwise prepared in an identical manner.

B. Dynamic light scattering

An ALV-5000 spectrometer-goniometer equipped with a digital correlator and a helium-neon laser (wavelength $\lambda=632.8$ nm) was used to measure the dynamics of the particles suspended in the Carbopol samples. All measurements were done at 25 °C. Dynamic light scattering (DLS) experiments measure the autocorrelation function $g^{(2)}(\tau)$ of the scattered intensity as a function of the delay or lag time τ. Most of our DLS experiments were made at a scattering angle of 30°, at which the scattering from the spheres was at least 10 times larger than that from the gel itself.

The measured quantity $g^{(2)}(\tau)$ is used to calculate the autocorrelation function of the scattered electric field $g^{(1)}(\tau)$ and the mean-squared displacement $\langle r^2(\tau)\rangle$. When the scattering of the electric field is a Gaussian process, the intensity and field autocorrelation functions are related through the Siegert relation [40]. However, the Carbopol samples, especially the more concentrated ones, are nonergodic because the spheres do not move enough to explore all possible configurations over the duration of the experiment. As a result, a simple time average of the particles' motion is not identical to an ensemble average. In this case, the calculation of $g^{(1)}(\tau)$ is more complicated [41]. We use the Schätzel formalism for nonergodic samples [42], modified to account for a finite detector area, to find the relation between $g^{(1)}(\tau)$ and $g^{(2)}(\tau)$:

$$g^{(1)}(\tau)=1+\frac{\langle I\rangle_T}{\langle I\rangle_E}\left[\sqrt{1+\frac{g^{(2)}(\tau)-g^{(2)}(0)}{\beta}}-1\right]. \quad (1)$$

Here $\langle I\rangle_T$ is the time average of the intensity obtained during a single measurement of $g^{(2)}(\tau)$ for a fixed sample orientation with respect to the laser beam. For a nonergodic sample, $\langle I\rangle_T$ will depend on orientation and $\langle I\rangle_E$ is the ensemble average of the intensity obtained by rotating the sample. β is a parameter that accounts for the finite area of our detector. It is obtained from the intercept of the ensemble average of $g^{(2)}(\tau)$—i.e., $\beta=\lim_{\tau\to0}[g_E^{(2)}(\tau)-1]$ where $g_E^{(2)}(\tau)$ is measured while the sample cell is rotated to average over different sample orientations. In our case, $\beta\approx0.35$. Note that Eq. (1) is also valid for ergodic samples, in which case $\langle I\rangle_T=\langle I\rangle_E$ and $g^{(2)}(0)=1+\beta$.

The mean-squared displacement can be calculated from $g^{(1)}(\tau)$ since [40]

$$g^{(1)}(\tau) = \exp\left[-\frac{q^2}{6}\langle r^2(\tau)\rangle\right], \tag{2}$$

where q is the magnitude of the scattering wave vector defined as $q=(4\pi n/\lambda)\sin(\theta/2)$, λ the vacuum wavelength of the incident light, n the refractive index of the medium, and θ the scattering angle. Accurate determination of $g^{(1)}(\tau)$ from $g^{(2)}(\tau)$ is difficult at large lag times, when $g^{(2)}(\tau)$ approaches its base-line value and the results become dominated by noise. In the present work, only data for which $g^{(2)}(\tau)-1 > 0.01$ are used.

C. Multiple-particle tracking

The motion of individual fluorescent polystyrene microspheres suspended in carbopol solutions was studied using an Olympus BX50Wi upright epi-illumination fluorescence microscope. Sample cells were made by gluing three small glass bars cut from a microscope slide onto a second slide with optical cement to form a U-shaped wall 10 mm $\times$ 10 mm $\times$ 0.75 mm high. A cover slip was then glued on top of this wall to form a chamber with one end open. Roughly 0.075 cm^3 of carbopol, prepared as above, was loaded into the chamber with a glass dropper, and the chamber was then sealed with a chemically inert silicone-based grease. The samples were allowed to equilibrate at room temperature for from 30 min to 1 h before measurements were made, and preliminary observations were made to ensure that there was no overall drift in the sample due to leaks in the sample chamber. The microscope was focused roughly halfway into the sample to minimize wall effects. The magnification of the optical system was 150×. At the particle concentration used, the microscope's field of view typically contained 50–100 particles at any time, but collisions between spheres were rare. Images of the spheres were captured with a charge-coupled-device (CCD) camera at a rate of 30 frames per second (fps) and recorded with a standard VCR for times ranging from 10 to 20 min, depending on the concentration of the sample. The recorded images were later digitized using a frame grabber in a personal computer. Images were digitized at frame rates ranging from 2 to 15 fps, chosen so that the motion of the spheres between frames was detectable by the particle-tracking software used. The amount of memory in our computer limited us to run lengths of 1800 frames, and for long runs the frame rate had to be reduced to compensate for this.

Image processing to determine the locations of the fluorescent particles in each video frame and analyze the particle trajectories was done using particle-tracking software written by Crocker and co-workers and described in detail in Refs. [43,44]. The scale of the images was calibrated using an etched calibration slide. Uncertainties in the particle positions due to the imaging system were determined by imaging immobile particles [45]. The accuracy of the tracking software and the experimental setup was verified by analyzing the motion of the fluorescent spheres in water under the same experimental conditions as used for the main experiments. While the light-scattering measurements give the mean-squared displacement in three dimensions, $\langle r^2\rangle$, the microscopy only allows measurement in the two-dimensional focal plane. In fact, since our system had higher spatial resolution in the x direction, we calculated a one-dimensional mean-squared displacement $\langle x^2\rangle$ and multiplied it by 3 for comparison with the light-scattering measurements. In doing so we are implicitly assuming that the Carbopol gels are isotropic.

D. Microrheology

The microscopic viscous and elastic moduli were determined from the mean-squared displacement using the method introduced by Mason [35]. It is based on the assumption that the Stokes-Einstein relation that is valid for Newtonian fluids can be generalized to viscoelastic fluids with frequency-dependent linear viscoelastic moduli and that inertial effects on the motion of the probe particles are negligible.

Following Mason, we define $\alpha(\omega)$ to be the logarithmic slope of the mean-squared displacement as a function of lag time τ,

$$\alpha(\omega) = \left.\frac{d\ln\langle r^2(\tau)\rangle}{d\ln\tau}\right|_{\tau=1/\omega}. \tag{3}$$

We then calculate the magnitude of the mechanical modulus

$$|G(\omega)| = \frac{k_B T}{\pi a\langle r^2(1/\omega)\rangle\Gamma(1+\alpha(\omega))}, \tag{4}$$

where k_B is the Boltzmann constant, T the temperature, a the particle radius, and Γ the gamma function. The viscous modulus G'' is given by

$$G''(\omega) = |G(\omega)|\sin\left(\frac{\pi\alpha(\omega)}{2}\right), \tag{5}$$

and the elastic modulus G' is

$$G'(\omega) = |G(\omega)|\cos\left(\frac{\pi\alpha(\omega)}{2}\right). \tag{6}$$

E. Bulk rheology

Bulk rheological measurements were made with an Ares RHS controlled strain rheometer. The sample was contained between parallel plates 5 cm in diameter. Fine sandpaper was glued to the surfaces of both plates to eliminate wall slip, and the gap between the plates was fixed at 1.0 mm. All measurements were made at a temperature of 25 °C. We performed both oscillatory and steady shear measurements. In the oscillatory measurements, a small, sinusoidally varying strain is applied to one plate and the resulting torque on the other plate is measured. The in-phase and out-of-phase components of the response give the elastic and viscous moduli G' and G'', respectively. The ratio of the moduli, $G''/G'=\tan\delta$, is the tangent of the phase angle δ between the applied strain and the measured stress. In the steady shear measurements, the steady-state stress σ is measured as a function of the applied steady shear rate $\dot{\gamma}$. The steady state was reached less than 10 s after the shear rate was imposed. Data were recorded by averaging for 60 s, starting 30 s after the onset of

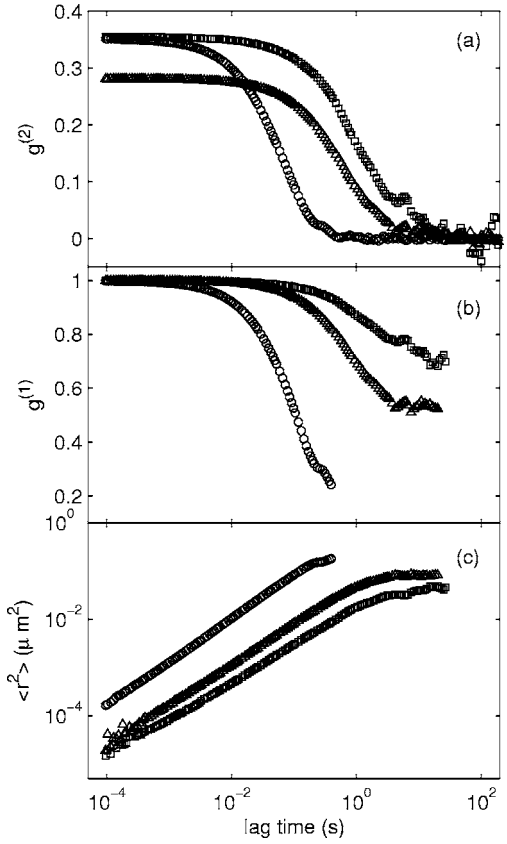

FIG. 1. (a) The intensity autocorrelation function $g^{(2)}(\tau)-1$ determined by dynamic light scattering from 0.49-μm spheres suspended in carbopol solutions. (b) The electric field autocorrelation function $g^{(1)}(\tau)-1$ determined from the data in (a) using Eq. (1). (c) The mean-squared displacement $\langle r^2(\tau)\rangle$ as a function of the lag time τ from the light scattering measurements. In all cases the different symbols indicate different Carbopol concentrations: 0.1 wt % (circles), 0.5 wt % (triangles), and 1 wt % (squares).

shear. In all cases the sample deformed uniformly under shear.

III. RESULTS

Figure 1 shows typical DLS results measured for three Carbopol samples of concentration 0.1, 0.5, and 1.0 wt %. The intensity correlation functions $g^{(2)}$ shown in Fig. 1(a) decay more slowly as the Carbopol concentration is increased. Variation in the $\tau=0$ intercept can also be observed in this graph; different intercepts were also observed each time the sample was rotated to a new position in the sample holder. These variations became larger as the concentration was increased, indicating that the samples became more nonergodic; the probe particles are not able to fully explore all possible environments. The field correlation functions $g^{(1)}$ calculated from these data are shown in Fig. 1(b). In all cases the low-τ intercept is one, but $g^{(1)}$ does not decay fully at large lag time because the samples are nonergodic.

The mean-squared displacements of the tracer particles in the different Carbopol samples are shown in Fig. 1(c). For lag times less than about 1 s, $\langle r^2(\tau)\rangle$ increases with a logarithmic slope α slightly less than the value of 1 expected for normal diffusion in a purely viscous medium. Fits to the data in the power law regime give logarithmic slopes α of 0.90, 0.83, and 0.78 for $c=0.1\%$, 0.5%, and 1%, respectively, indicating that the particle motion over these short time scales is slightly subdiffusive and becomes more so as the concentration increases. At any particular lag time, the mean-squared displacement drops by more than one order of magnitude as the gel concentration increases from 0.1 to 1.0 wt %. At higher lag times α becomes dependent on τ and $\langle r^2(\tau)\rangle$ starts to level off, indicating that the motion of the particles becomes more restricted as they explore more of the material.

At the largest lag times probed by the DLS measurements, the mean-squared displacement plateaus at a concentration-dependent value. It is important to note that these plateaus occur at lag times at which the intensity correlation function has almost fully decayed. At these lag times, the correlation functions are noisy and decay slowly. This slow decay could be due, for example, to correlations from particles that are moving very slowly and have not moved far enough for the scattered light to be decorrelated. If this were the case, this part of the correlation function should become less noisy for longer measurements where more slow particles can be measured. Alternatively, this slow decay could be due to aging [46] or rearrangement of the carbopol particles. In this case the signal would remain noisy as the structure evolves. In our case data were collected in runs of 10 min duration and longer runs did not make the signal less noisy, so the latter scenario is more likely.

Light-scattering experiments were also performed with particles having diameters ranging from 200 to 630 nm. For unhindered diffusion, one would expect $\langle r^2(\tau)\rangle \propto 1/a$. This is approximately true over the range of τ accessible to DLS, although the scaled data have slightly different values of the logarithmic slope α.

Figure 2(a) shows typical individual particle trajectories measured by fluorescence microscopy particle tracking for three concentrations of carbopol. At a concentration of 0.01% (not shown), the motion of the particles is indistinguishable from Brownian diffusion. At $c=0.1\%$, as shown in Fig. 2(a), the particle appears to stay in one region for a period of time and then jump to another region. This behavior is much more pronounced at $c=0.5\%$, while at 1% the particles move very little [47].

The one-dimensional mean-squared displacements $\langle x^2(\tau)\rangle$ determined from the particle-tracking experiments are shown in Fig. 2(b) for $c=0.1\%$, 0.5%, and 1%. At $c=0.01\%$ (not shown) $\langle x^2(\tau)\rangle$ increases linearly with lag time τ. For higher concentrations, the motion is subdiffusive. Fits to the data in the range $1\leqslant\tau\leqslant 10$ s give logarithmic slopes of 0.78, 0.59, and 0.31 for $c=0.1\%$, 0.5%, and 1.0% by weight, respectively. As for the light-scattering data, the subdiffusive increase of the mean-squared displacement indicates that the motion of the particles is constrained by the presence of structure in the gel, but the effect is evidently more significant at the longer lag times probed by the particle-tracking experiments. Additional experiments using 1.0-μm beads show that $\langle x^2(\tau)\rangle \propto 1/a$ for $c=0.01\%$, but this scaling does

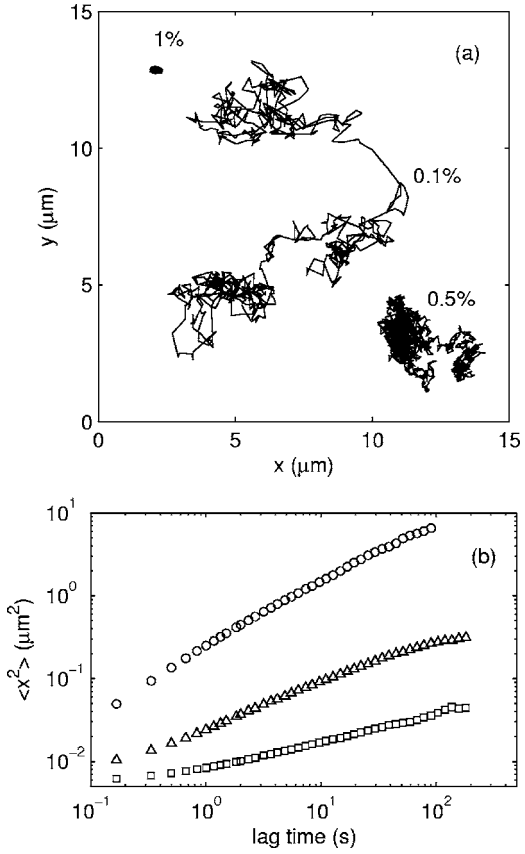

FIG. 2. (a) Typical trajectories of 0.49-μm fluorescent particles suspended in carbopol solutions, measured by fluorescence microscopy particle tracking. Trajectories for three different concentrations are shown. (b) The mean-squared displacement $\langle x^2(\tau)\rangle$ determined from analysis of the x components of the trajectories of many particles. The symbols indicate different concentrations as in Fig. 1.

not apply at higher concentrations, indicating that over the time scales relevant to the particle-tracking experiments, the particles move distances comparable to the length scale of the structure of the gel [16].

In Fig. 3 we plot the values of $\langle r^2(\tau)\rangle$ from both the light-scattering and particle-tracking experiments. The three sets of data are for three different concentrations and are offset vertically for clarity. The data from the two different experiments are completely consistent and probe complementary time and distance scales. Taken together, they cover at least six orders of magnitude in τ. The data at the low-τ end of the particle-tracking results are slightly higher than the corresponding light-scattering data at high concentrations. This is because these data are close to the spatial resolution of the particle-tracking experiment and so are affected by noise. The dashed curves drawn through the data in Fig. 3 are fits to the empirical functional form

$$\langle r^2(\tau)\rangle = A\left[\left(\frac{\tau}{\tau_0}\right)^{\alpha_1} + \left(\frac{\tau}{\tau_0}\right)^{\alpha_2}\right]^{-1} \tag{7}$$

and are intended simply to provide a convenient parametrization of the data.

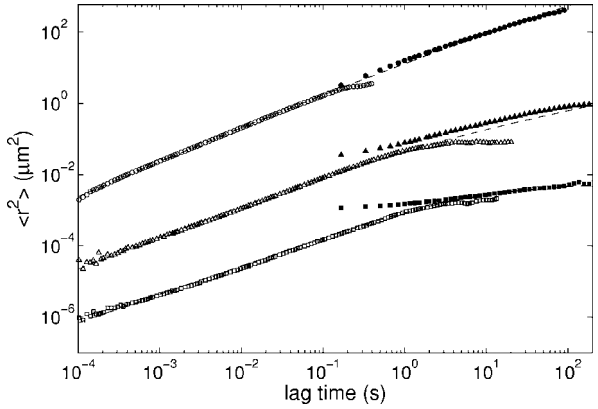

FIG. 3. A comparison of the data for $\langle r^2(\tau)\rangle$ from both light-scattering and particle-tracking measurements. The data shown are for concentrations of 0.1% (circles), 0.5% (triangles), and 1% (squares). Light-scattering data at lower τ are shown as open symbols. The solid symbols at higher τ are data from particle-tracking measurements. The dashed lines are smooth curves drawn through the data to parametrize them, as discussed in the text. For clarity, the data for $c=0.1\%$ and 1% have been shifted upwards and downwards by a factor of 20 in $\langle r^2(\tau)\rangle$, respectively.

The moduli calculated from the fits to Eq. (7) using Eqs. (5) and (6) are shown in Fig. 4, where the heavy lines indicate G' and the lighter lines G''. The different line styles show the results for the different concentrations. At $c=1\%$ the elastic modulus G' dominates at low frequencies, and there is a crossover frequency above which the viscous modulus becomes dominant. This crossover frequency apparently decreases as the concentration decreases, and for $c=0.1\%$ and 0.5% the viscous modulus is larger than the elastic modulus over the range of frequencies covered by our experiments.

For comparison, the bulk viscoelastic moduli measured with the shear rheometer are shown as symbols in Fig. 4. The

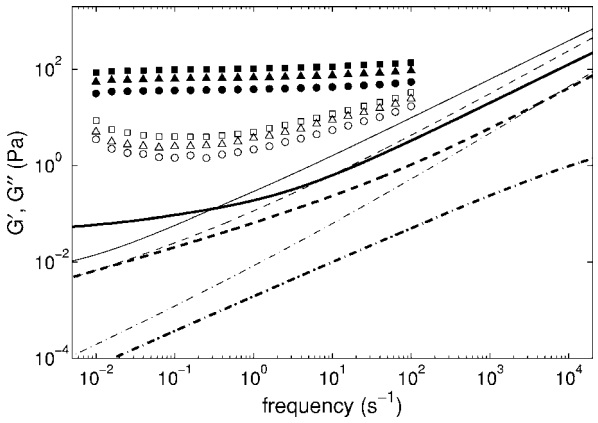

FIG. 4. The elastic modulus G' and viscous modulus G'' as a function of frequency. The moduli determined from the curves through the data shown in Fig. 3 are shown as heavy (G') and light (G'') lines, with dash-dotted lines representing $c=0.1\%$; dashed lines, $c=0.5\%$; and solid lines, $c=1\%$. The symbols are bulk values, measured with a shear rheometer, with solid symbols representing G' and open symbols G''. The different symbols indicate the different concentrations as in previous figures.

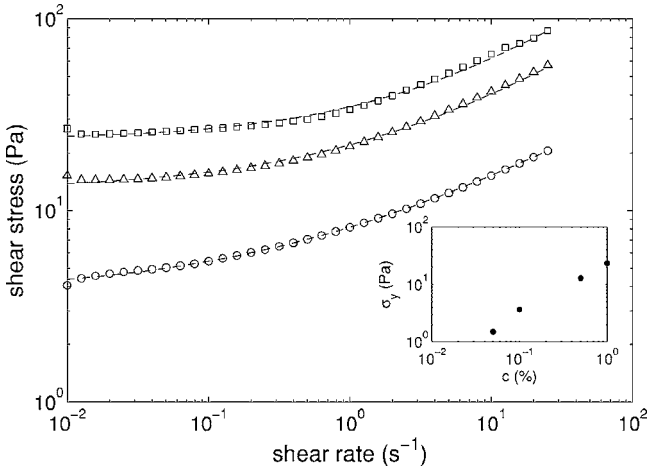

FIG. 5. The shear stress as a function shear rate under steady shear (flow curve) for three concentrations of Carbopol. As before, the concentrations are 0.1% (circles), 0.5% (triangles), and 1% (squares). The dashed lines are fits of the data to a Herschel-Bulkley constitutive relation. In all cases this form describes the data well. The inset shows the yield stress determined from these fits as a function of concentration.

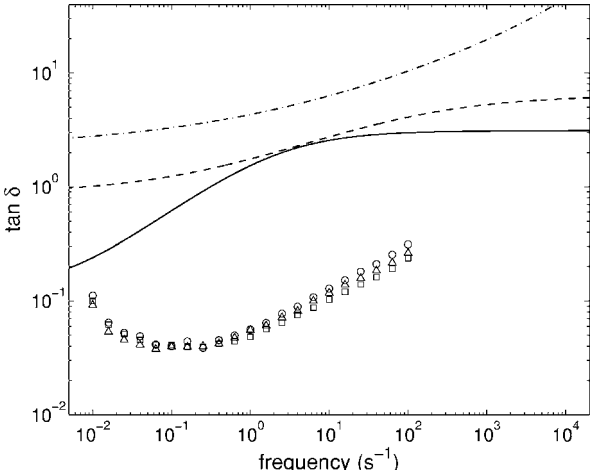

FIG. 6. The quantity tan $\delta = G''/G'$ determined from both microrheological and bulk measurements. The lines and symbols have the same meaning as in Fig. 4.

bulk results give moduli that are orders of magnitude larger than those determined from the microrheological measurements, and in contrast to the microrheological results, the bulk value of G' is always significantly larger than G'' over the range of shear rates accessible to our instrument.

Figure 5 shows flow curves measured with the rheometer for three concentrations. In all three cases, the flow curves approach a constant stress at low shear rates, indicating the presence of a yield stress. The lines through the data in Fig. 5 are fits to a Herschel-Bulkley constitutive relation [48],

$$\sigma = \sigma_y + K\dot{\gamma}^n, \tag{8}$$

where σ_y is the yield stress, K is the consistency, and n is a power law index. This model fits our data well. Our fits gave $n=0.40$, 0.48, and 0.53 for $c=0.1\%$, 0.5%, and 1.0%, respectively. The yield stress determined from these fits is shown as a function of concentration in the inset to Fig. 5; it increases roughly linearly with concentration over the range studied.

Figure 6 shows tan $\delta = G''/G'$ for both the microrheological and bulk results. In the bulk case, tan δ is small, being less than 0.1 over most of the applicable frequency range. This indicates that, on large length scales, the response of the material to small strains is almost entirely elastic. This is a result of the yield stress: at low frequencies and for values of the shear stress smaller than the yield stress, the gels behave as soft elastic solids. On the other hand, the microscopic values of tan δ are much larger, with tan $\delta > 1$ at all frequencies for $c=0.1\%$ and 0.5% and at high frequencies for the highest concentration. This indicates that the microscopic-scale response of the material to the motion of the small tracer particles is much more like that of a viscous fluid than an elastic solid.

The dynamic viscosity η is given by G''/ω. In Fig. 7 we plot the viscosities obtained from both the bulk and microrheological viscous moduli. The bulk viscosities diverge approximately as ω^{-1} as ω decreases, as expected for a yield-stress fluid. The microscopic viscosities also appear to diverge at low frequencies, but more slowly than ω^{-1}, and are at least two orders of magnitude smaller than the bulk values. The bulk and microscopic values appear to be approaching each other at high frequencies, where the microscopic viscosities approach a concentration-dependent constant value which is roughly four times that of water for $c=0.1\%$.

IV. DISCUSSION

The results obtained for the mean-squared displacements from the light-scattering and particle-tracking experiments show good agreement and cover complementary ranges of lag time. The logarithmic slope of the mean-squared displacement is slightly less than unity, and $\langle r^2(\tau)\rangle$ scales with particle size at short lag times. At longer times the slope decreases. This behavior is similar to that reported in Ref.

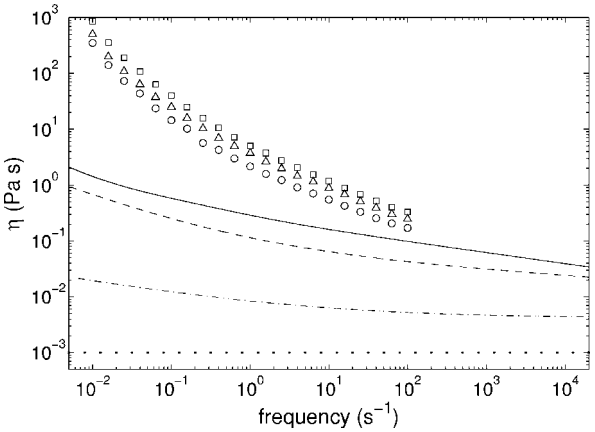

FIG. 7. The dynamic viscosity as determined from both bulk (symbols) and microrheological (curves) measurements for the three concentrations studied. The symbols and curves are associated with the different concentrations as in Fig. 4. The heavy dotted line represents the viscosity of water.

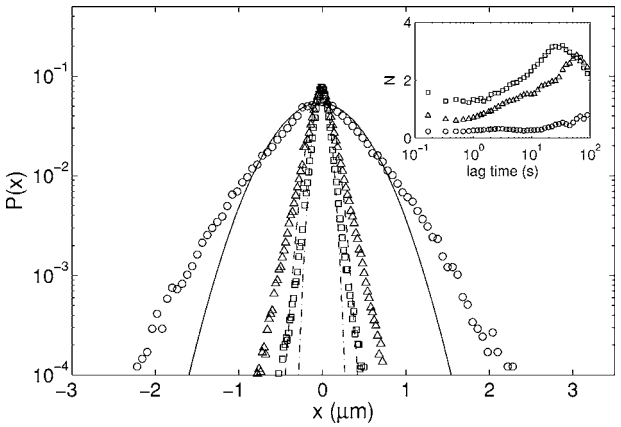

FIG. 8. The probability $P(x)$ that a particle moves a distance x in lag time τ. Here $\tau=10$ s. The symbols indicate different concentrations as in the previous figures. The curves are the best-fit Gaussian distributions for each data set: dot-dashed lines, 0.1 wt %; dashed lines, 0.5 wt %; and solid lines, 1 wt %. These fits clearly do not describe the data well. The inset shows the non-Gaussian parameter defined in the text as a function of τ for the same three concentrations.

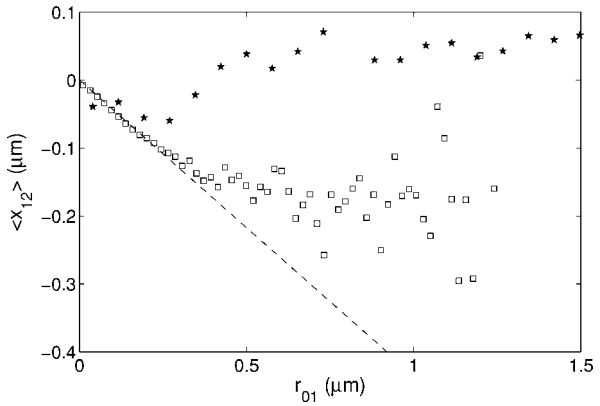

FIG. 9. A plot showing the degree of correlation between subsequent particle displacements for a lag time $\tau=10$ s, as described in the text. The solid stars are from particle tracking measurements with $c=0.01\%$ and show a correlation close to zero. At higher concentration (the squares are for $c=1\%$), there is a negative correlation between subsequent displacements, indicating the importance of caging effects on the particle motion.

[16], in which the motion of tracer particles in entangled F-actin networks was studied. It was observed that when the particle size was much less than the mesh size of the polymer network, the particle motion measured an average viscosity of the medium. When the particle size was comparable to mesh size, the motion became subdiffusive as the particles became trapped in the network and sampled different microrheological environments within the material.

The data for $\langle x^2(\tau)\rangle$ plotted in Fig. 2 are averaged over all particles, just as the light-scattering data are, and over all starting times. Examination of individual trajectories shows that at the higher concentrations there is a strong variation in $r^2(\tau)$ from particle to particle—some particles are completely trapped and do not move at all, while others move further [47]—evidence that the Carbopol is inhomogeneous and made up of different microscopic rheological environments. The extent of this behavior is illustrated in Fig. 8, which shows the probability distribution of particle step sizes, known as the van Hove correlation function, for $c=0.1\%$, 0.5%, and 1%. For Brownian diffusion, one expects a Gaussian distribution, and this is observed for $c=0.01\%$. For the concentrations shown in Fig. 8, however, the distributions are strongly non-Gaussian due to the inhomogeneity of the material. This can be quantified using a "non-Gaussian parameter" which measures the deviations of the distribution from Gaussian [49]:

$$N=\frac{\langle x^4\rangle}{3\langle x^2\rangle^2}-1. \tag{9}$$

This quantity is zero for a Gaussian distribution, while a positive value indicates a distribution that is sharper and more peaked than a Gaussian. N is plotted as a function of lag time for three concentrations in the inset to Fig. 8. This graph shows that the motion of the particles becomes more strongly affected by the gel structure as τ increases, reaching a maximum at a lag time that appears to decrease with increasing concentration. The decrease in N seen at high τ suggests that over longer times the gel structure slowly evolves or the particles escape from the traps.

The data in Figs. 2 and 8 show that the motion of the particles in the Carbopol is restricted—that is, that the particles are to some extent trapped in cages resulting from the structure of the fluid. The trapping picture is confirmed by Fig. 9, which shows how the motion of a particle at time $t_1=t_0+\tau$ is correlated with that at time t_0 [50,51]. Consider a particle that moves a two-dimensional displacement $\vec{r}_{01}$ in the focal plane between t_0 and t_1. If the motion of the particle is a random walk, then the direction of the displacement $\vec{r}_{12}$ in the next time interval will be uncorrelated with that of $\vec{r}_{01}$. On the other hand, if the particle is trapped in a cage, it may approach the wall of the cage during the first interval, then bounce off and move away from the wall in the next interval. In this case one would expect $\vec{r}_{12}$ to be oriented preferentially in the opposite direction to $\vec{r}_{01}$. In Fig. 9 we plot the distance r_{01} on the horizontal axis and $\langle x_{12}\rangle$, the mean of the projection of $\vec{r}_{12}$ in the direction of $\vec{r}_{01}$, on the vertical axis. For $c=0.01$, for which the motion is diffusive, there is no correlation—$\langle x_{12}\rangle$ is independent of the size of the previous step. For higher concentrations, in contrast, there is a strong negative correlation, indicative of caging effects. The slope of the linear region at low r_{01} is related to the logarithmic slope of $\langle r^2(\tau)\rangle$ [50,51] and is a measure of the strength of the cage, while r^*, the value of r_{01} at which the negative correlation starts to break down, is a measure of the size of the pores in which the particles are trapped. The pore size δ is approximately $2a+r^*$, where a is the particle radius; we find $\delta=0.76$ μm for $c=0.5\%$ and 1% and $\delta=1.8$ μm for $c=0.1\%$.

The behavior we observe is consistent with the commonly accepted model for the structure of Carbopol gels, as sketched in Fig. 10 [8,9]. The swollen Carbopol particles consist of concentrated centers of strongly cross-linked polymer molecules surrounded by regions of more dilute polymer

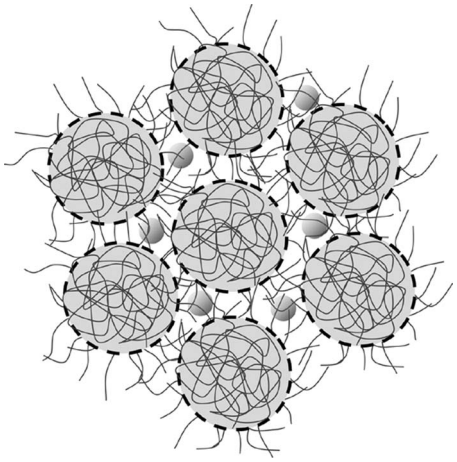

FIG. 10. A schematic illustration of the structure of Carbopol gels showing the highly cross-linked cores of the microgel particles surrounded by a viscous medium containing polymer chains (after Ref. [9]). The small probe particles diffuse in the pores of viscous fluid between the gel particles.

solution. We interpret our results as indicating that the tracer particles diffuse in the viscous polymer solution between the denser microgel cores. The cores themselves restrict the motion of the tracers, leading to the observed subdiffusive behavior. At higher concentrations the dense cores become more closely packed, effectively trapping the particles in micron-sized pores between the microgel cores. More detailed structural information could be obtained from neutron- or x-ray-scattering experiments. Our preliminary small-angle neutron-scattering results show no evidence for a characteristic length scale—the scattered intensity simply falls off as $1/q^2$, where q is magnitude of the neutron-scattering wave vector.

The bulk rheological data presented in Figs. 4 and 5 show yield-stress behavior. The flow curves flatten out to a constant stress at low shear rates, and the elastic modulus dominates over the range of frequencies covered for all concentrations. In contrast, the microrheological results show that at small scales the viscous modulus dominates over most of the frequency and concentration range studied and that both the elastic and viscous moduli are much smaller than results from bulk rheometry. Thus the microscopic environment sampled by the particles is primarily viscous, while the bulk response is primarily elastic. The microrheological dynamic viscosity shown in Fig. 7 increases as the frequency decreases, although the divergence is considerably slower than the ω^{-1} dependence observed on the bulk scale in yield-stress fluids. This behavior is also in contrast to what is typically observed in polymer solutions, for which the viscosity is constant at low frequencies.

V. CONCLUSION

We have used dynamic light scattering and particle tracking to determine the mean-squared displacement of fluorescent tracer particles suspended in Carbopol gels. From our results we have calculated the microscopic viscoelastic moduli. At the shortest time scales probed by our measurements, the particles move in a primarily viscous medium, while at longer times the elastic modulus is more evident, dominating over the viscous modulus at high Carbopol concentration. Viscous and elastic moduli measured using a shear rheometer are orders of magnitude larger than the microrheological data. These results, as well as more detailed analysis of the particle-tracking data, are consistent with the material being heterogeneous on the length scale of the particles, so that the individual particles probe a variety of microscopic rheological environments and can become trapped by pores in the gel. Flow curves measured with the shear rheometer indicate the presence of a yield stress on the macroscopic scale. On the microscopic scale the elastic modulus becomes dominant and the viscosity increases as the time scale increases, but the increase is slower than that observed in the bulk scale.

ACKNOWLEDGMENTS

This research was supported by the Canadian Space Agency and the Natural Science and Engineering Research Council of Canada. We acknowledge helpful discussions with D. Weitz, technical assistance from M. Goldsworthy, the use of a rheometer from I. Frigaard, and assistance with preliminary experiments from R. McKenzie.

[1] R. G. Larson, *The Structure and Rheology of Complex Fluids* (Oxford University Press, New York, 1999).
[2] Noveon technical data sheet No. 216, www.pharma.noveon.com/literature/tds/tds216.pdf
[3] S. J. Curran, R. E. Hayes, A. Afacan, M. C. Williams, and P. A. Tanguy, J. Food. Sci. **67**, 176 (2002).
[4] L. Jossic and A. Magnin, AIChE J. **47**, 2666 (2001).
[5] D. D. Atapattu, R. P. Chhabra, and P. H. T. Uhlherr, J. Non-Newtonian Fluid Mech. **38**, 31 (1990); **59**, 245 (1995).
[6] N. W. Taylor and E. B. Bagley, J. Appl. Polym. Sci. **18**, 2747 (1974).
[7] R. J. Ketz, Jr., R. K. Prud'homme, and W. W. Graessley, Rheol. Acta **27**, 531 (1988).
[8] J. O. Carnali and M. S. Naser, Colloid Polym. Sci. **270**, 183 (1992).
[9] G. P. Roberts and H. A. Barnes, Rheol. Acta **40**, 499 (2001).
[10] L. Baudonnet, J. L. Grossiord, and F. Rodriguez, J. Dispersion Sci. Technol. **25**, 183 (2004).
[11] J.-Y. Kim, J.-Y. Sing, E.-J. Lee, and S.-K. Park, Colloid Polym. Sci. **281**, 614 (2003).
[12] F. C. MacKintosh and C. F. Schmidt, Curr. Opin. Colloid Interface Sci. **4**, 300 (1999).
[13] M. J. Solomon and Q. Lu, Curr. Opin. Colloid Interface Sci. **6**, 430 (2001).

[14] T. A. Waigh, Rep. Prog. Phys. **68**, 685 (2005).
[15] M. L. Gardel, M. T. Valentine, and D. A. Weitz, in *Microscale Diagnostic Techniques*, edited by K. Breuer (Springer, New York, 2005).
[16] I. Y. Wong, M. L. Gardel, D. R. Reichman, E. R. Weeks, M. T. Valentine, A. R. Bausch, and D. A. Weitz, Phys. Rev. Lett. **92**, 178101 (2004).
[17] B. R. Dasgupta, S.-Y. Tee, J. C. Crocker, B. J. Frisken, and D. A. Weitz, Phys. Rev. E **65**, 051505 (2002).
[18] T. G. Mason and D. A. Weitz, Phys. Rev. Lett. **74**, 1250 (1995).
[19] T. G. Mason, H. Gang, and D. A. Weitz, J. Mol. Struct. **383**, 81 (1996).
[20] T. Gisler and D. A. Weitz, Phys. Rev. Lett. **82**, 1606 (1999).
[21] T. G. Mason, K. Ganesan, J. H. van Zanten, D. Wirtz, and S. C. Kuo, Phys. Rev. Lett. **79**, 3282 (1997).
[22] Y. Tseng and D. Wirtz, Biophys. J. **81**, 1643 (2001).
[23] M. T. Valentine, P. D. Kaplan, D. Thota, J. C. Crocker, T. Gisler, R. K. Prud'homme, M. Beck, and D. A. Weitz, Phys. Rev. E **64**, 061506 (2001).
[24] M. L. Gardel, M. T. Valentine, J. C. Crocker, A. R. Bausch, and D. A. Weitz, Phys. Rev. Lett. **91**, 158302 (2003).
[25] F. Zeimann, J. Radler, and E. Sackmann, Biophys. J. **66**, 2210 (1994).
[26] F. G. Schmidt, F. Ziemann, and E. Sackmann, Eur. Biophys. J. **24**, 348 (1996).
[27] F. Amblard, A. C. Maggs, B. Yurke, A. N. Pargellis, and S. Leibler, Phys. Rev. Lett. **77**, 4470 (1996).
[28] M. T. Valentine, L. E. Dewalt, and H. D. Ou-Yang, J. Phys.: Condens. Matter **8**, 9477 (1996).
[29] H. D. Ou-Yang, in *Colloid-Polymer Interactions: From Fundamentals to Practice*, edited by R. S. Farinato and P. L. Dubin (Wiley, New York, 1999).
[30] S. Hénon, G. Lenormand, A. Richert, and F. Gallet, Biophys. J. **76**, 1145 (1999).
[31] J. Sleep, D. Wilson, R. Simmons, and W. Gratzer, Biophys. J. **77**, 3085 (1999).
[32] K. C. Neuman and S. M. Block, Rev. Sci. Instrum. **75**, 2787 (2004).
[33] B. Schnurr, F. Gittes, F. C. MacKintosh, and C. F. Schmidt, Macromolecules **30**, 7781 (1997).
[34] F. Gittes, B. Schnurr, P. D. Olmsted, F. C. MacKintosh, and C. F. Schmidt, Phys. Rev. Lett. **79**, 3286 (1997).
[35] T. G. Mason, Rheol. Acta **39**, 371 (2000).
[36] B. R. Dasgupta and D. A. Weitz, Phys. Rev. E **71**, 021504 (2005).
[37] Q. Lu and M. J. Solomon, Phys. Rev. E **66**, 061504 (2002).
[38] M. Cloitre, R. Borrega, F. Monti, and L. Leibler, Phys. Rev. Lett. **90**, 068303 (2003).
[39] Duke Scientific Inc., www.dukescientific.com
[40] B. J. Berne and R. Pecora, *Dynamic Light Scattering: With Applications to Chemistry, Biology, and Physics* (Wiley, New York, 1976).
[41] P. N. Pusey and W. van Megen, Physica A **157**, 705 (1989); J. G. H. Joosten, E. T. F. Geladé, and P. N. Pusey, Phys. Rev. A **42**, 2161 (1990).
[42] K. Schätzel, Appl. Opt. **32**, 3880 (1993).
[43] J. C. Crocker and D. G. Grier, J. Colloid Interface Sci. **179**, 298 (1996).
[44] E. Weeks and J. C. Crocker, Particle tracking using IDL, http://www.physics.emory.edu/~weeks/idl/.
[45] D. S. Martin, M. B. Forstner, and J. A. Kas, Biophys. J. **83**, 2109 (2002).
[46] P. Sollich, F. Lequeux, P. Hébraud, and M. E. Cates, Phys. Rev. Lett. **78**, 2020 (1997).
[47] F. Oppong and J. R. de Bruyn (unpublished).
[48] R. W. Whorlow, *Rheological Techniques* (Ellis Horwood, New York, 1992).
[49] W. K. Kegel and A. van Blaaderen, Science **287**, 290 (2000).
[50] B. Doliwa and A. Heuer, Phys. Rev. Lett. **80**, 4915 (1998); J. Phys.: Condens. Matter **11**, A277 (1999).
[51] E. R. Weeks and D. A. Weitz, Chem. Phys. **284**, 361 (2002); Phys. Rev. Lett. **89**, 095704 (2002).